



Reduced graphene oxide/ZnO nanocomposite modified electrode for the detection of tetracycline

Ana Đurović¹, Zorica Stojanović^{1,*}, Zuzana Bytešníková², Snežana Kravić¹, Pavel Švec², Jan Příbyl³, and Lukáš Richtera^{2,4}

¹ Faculty of Technology Novi Sad, University of Novi Sad, Bulevar cara Lazara 1, 21000 Novi Sad, Serbia

² Department of Chemistry and Biochemistry, Mendel University in Brno, Zemědělská 1, 613 00 Brno, Czech Republic

³ CEITEC MU, Masaryk University, Kamenice 5/A35, 62 500 Brno, Czech Republic

⁴ Central European Institute of Technology, Brno University of Technology, Purkyňova 656/123, 612 00 Brno, Czech Republic

Received: 28 September 2021

Accepted: 14 January 2022

Published online:
21 February 2022

© The Author(s), under exclusive licence to Springer Science+Business Media, LLC, part of Springer Nature 2022

ABSTRACT

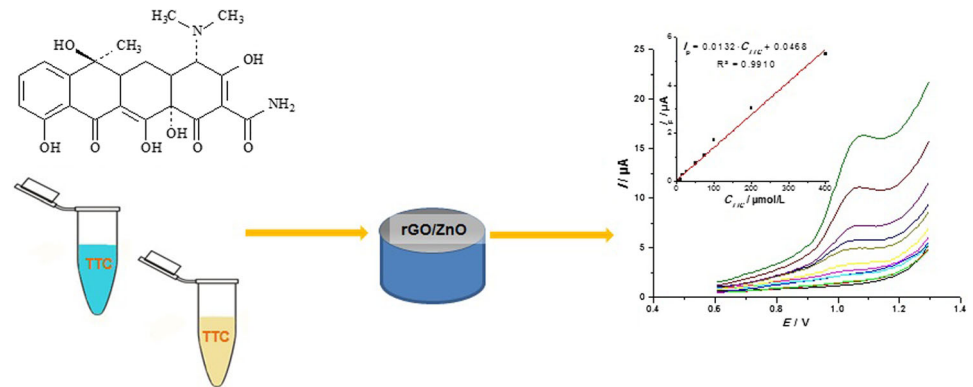
In this work, rGO-ZnO (reduced graphene oxide–zinc oxide) nanocomposite was prepared and used for modification of GC (glassy carbon) surface in order to obtain an electrochemical sensor for tetracycline determination in water and urine samples by voltammetric technique. The characterization of synthesized nanocomposite was accomplished by utilizing SEM, EDS, AFM and FTIR analyses. The electrochemical behaviour of tetracycline on the modified GCE was studied by cyclic voltammetry and results revealed that modification enhanced the electro-oxidation of tetracycline with increased current intensity. Tetracycline provided a well-defined oxidation peak at around + 1.05 V *vs.* Ag/AgCl (3.5 mol/L KCl) in Britton–Robinson buffer (BRB) at pH 8.0. Then, square-wave voltammetry (SWV) was applied for analytical purposes. The influence of the supporting electrolyte (type, concentration and pH) and SWV parameters on the peak current was investigated in order to optimize the experimental and instrumental conditions for quantitative analysis. Under the optimal conditions, the prepared sensor exhibits a wide linear range (4–400 μmol/L) with a low limit of detection (0.38 μmol/L) and good reproducibility of analysis (RSD < 3.40%). In addition, the sensor showed high selectivity towards tetracycline analysis in comparison to interferences often present in real samples. The practical analytical usefulness of the presented sensing platform was successfully demonstrated in the determination of tetracycline in water and human urine with good recoveries.

Handling Editor: Joshua Tong.

Address correspondence to E-mail: zorica.stojanovic@uns.ac.rs

<https://doi.org/10.1007/s10853-022-06926-1>

GRAPHICAL ABSTRACT



Introduction

Due to extensive usage, and daily discharge into the environment, pharmaceuticals have been recognized as emerging contaminants worldwide. Among them, antibiotics are one of the most commonly used pharmaceutical substances. Tetracyclines (TCs) are a group of antibiotics derived from *Streptomyces* with a broad-spectrum activity against a wide range of bacteria, including atypical organisms, such as *Chlamydiae*, *Mycoplasmataceae*, and *Rickettsiae* [1]. Additionally, they were used for protozoan parasites, prophylactically for the prevention of malaria [1], and at subtherapeutic levels for treatment of a variety of non-infectious conditions [2]. Since the introduction of TCs, these compounds were rapidly gaining wonder-drug status owing to their low price and the ability to inhibit the growth of a broad range of bacteria [1, 3]. Besides antibiotic activity and protein-synthesis inhibition, there were reports about their immunosuppressive effects as well [3]. Apart from wide application in human and animal medicine, TCs are also used as growth promoters in animal feed, increasing thus nutrient uptake efficiency and commercial benefit for farmers [1, 4]. TCs family includes natural products: oxytetracycline, tetracycline and demeclocycline, and semi-synthetic tetracyclines: minocycline and doxycycline, which are the most widely used [3].

Many antibiotics are not completely metabolized during use, or poor body adsorption occurs, while the rest is excreted in the environment [5, 6]. Thus, the excessive use of TCs over the years has led to contamination of food, environmental water, soils and sediments having thus deleterious consequences for human health [7–9]. Some of the negative effects related to excessive exposure to these substances include allergic reactions, liver damage, gastrointestinal disturbances, teratogenicity, teeth discoloration, with an inevitable increase in the pathogens population resistance to these drugs and a negative impact on the local biota [7, 8, 10]. Therefore, the development of rapid and easily applicable analytical methods suitable for the selective determination of TCs is of exceptional importance. Different methods are reported for the determination of tetracycline (TC), as a representative member of the TCs group, in real samples. The most conventional methods are based on chromatography, including high-performance liquid chromatography (HPLC) [11–13], and liquid chromatography (LC) [14, 15]. Capillary electrophoresis [16] and enzyme-linked immunosorbent assay are established as well [17]. Nevertheless, many drawbacks are associated with the practical utility of these methods, such as complicated and time-consuming sample preparation procedures, expensive equipment, and the necessity of well-trained scientific staff. Nowadays, analysts require the development of simple and fast methods, easily applicable to different real samples, without everlasting sample

preparation procedures. Recently, analytical methods based on electrochemistry arouse great interest among scientists, due to their simple operation, rapid response and low toxic chemicals consumption, providing thus a promising approach for TC determination in a complex matrix. The electroanalytical determination of TC in real samples is reported, including amperometric [18] and voltammetric methods [19–26]. The most commonly used strategy for developed methodologies is based on the use of differently modified glassy carbon electrodes [18, 21–24], in order to improve the performance of the developed methods in relation to bare glassy carbon electrode (GCE). The applications of the modified carbon paste electrode [25] and graphite-polyurethane composite electrode [19, 20] have also been reported.

Graphene is the most attractive nanomaterial built of a two-dimensional allotrope of carbon with a planar honeycomb lattice [27]. Owing to its unique structure, graphene is distinguished with astonishing mechanical strength, a high surface to volume ratio, unique electronic and mechanical properties and good chemical stability and thermal conductivity [28], but due to its high cost and lack of manufacturing scalability is not readily used as the basis of electrochemical sensors in a form of clearly pristine [29]. Consequently, other derivatives of graphene such as graphene oxide (GO) and reduced graphene oxide (rGO) are explored and widely utilized. In electrochemical sensing, GO is difficult to use alone for modifying electrodes due to the electrically insulating properties [30]. However, rGO possesses properties closer to those of pristine graphene, with a minimized number of oxygen groups, and it is usually fabricated by the process of oxidation, or exfoliation of graphite to GO, and then its reduction can be performed via chemical, thermal, or electrochemical routes [29]. Therefore, the use of rGO is reported to increase the sensor's performance throughout an increased area and high electro-conductivity, and it has been utilized in many electrochemical sensing applications [28, 31]. rGO has been combined with different material entities such as metal, metal oxide, biomolecules and polymers, and the obtained nanocomposites can combine the individual advantages of each component, thus demonstrating improved performance [32, 33]. More recently, ZnO as a material has significantly attracted the attention of scientists. It is a semiconductor characterized by

the high photoelectric reaction, admirable chemical and thermal stability and non-toxic nature, enabling it to be an integral part of highly selective and sensitive sensors and biosensors, as well. In electrochemical sensing, it has exhibited potent catalytic performance for analysis of various analytes. Nanostructured ZnO is widely used for the detection of various substances, including drugs [34], dyes [35] and selenium [36]. Moreover, in combination with graphene oxide, ZnO showed even improved electrocatalytic performance [33, 35, 37]. In view of this, we have combined these two materials in order to develop a rGO-ZnO nanocomposite modified glassy carbon electrode (rGO-ZnO-GCE), as an electrochemical sensing platform for selective and sensitive determination of TC using square wave voltammetry (SWV) as a detection technique. After optimization and validation, developed voltammetric methodology was successfully employed for the direct determination of TC in water and urine samples.

Experimental

Reagents and instrumentation

Tetracycline hydrochloride (95%) powder, ZnO nanopowder and $K_3[Fe(CN)_6]$, $K_4[Fe(CN)_6]$ were purchased from Sigma Aldrich (St. Louis, MO, USA). A stock solution of TC (2 mmol/L) was prepared by dissolving the substance in 0.01 mol/L HCl (Merck, Darmstadt, Germany). As a supporting electrolyte, a Britton–Robinson buffer (BRB) (0.1 mol/L, pH 8.0) was used. The buffer was prepared by mixing the equimolar amount of acetic, boric and phosphoric acid. The required pH value of the buffer was adjusted by the addition of sodium hydroxide solution (5 mol/L). Acids used for the preparation of the BRB (acetic, boric and phosphoric acid) and sodium hydroxide were purchased from Lach-Ner (Brno, Czech Republic). All solutions were prepared using double distilled water obtained using MonoDest 3000 E system (Brand, Wertheim, Germany).

Voltammetric measurements were conducted using a PalmSens4 potentiostat (PalmSens BV, GA Houten, Netherlands) operated by PStace software (version 5.4). A three-electrode assembly cell consisted of bare or modified glassy carbon disc electrode (3 mm, CHI 104, CHI Instruments, Austin, USA) as a working electrode, platinum wire as a

counter electrode, and an Ag/AgCl (3.5 mol/L, KCl) as a reference electrode. For pH adjustments, a previously two-point calibrated pH meter (HI 9321, Hanna Instruments, Woonsocket, RI, USA) equipped with pH electrode (HI1090B/5, Hanna Instruments, Woonsocket, RI, USA) was used.

Preparation of the rGO-ZnO

GO was prepared by chemical oxidation of 5 g graphite flakes (100 mesh, $\geq 75\%$ min) (Sigma Aldrich, St. Louis, MO, USA) in a mixture of concentrated H_2SO_4 (670 mL) (Penta, Prague, Czech Republic) and 30 g KMnO_4 (Sigma Aldrich, St. Louis, MO, USA) according to the simplified Hummers' method [38]. The reaction mixture was stirred vigorously. After 10 days, the oxidation of graphite was terminated by the addition of H_2O_2 solution (250 mL, 30 wt %) (Penta, Prague, Czech Republic). Formed GO was washed 3 times with 1 mol/L HCl (37 wt %) (Penta, Prague, Czech Republic) and several times with double distilled water (total volume approximately 10 L) until constant pH value (3–4) was achieved.

The volume of 1 mL of GO dispersion (5 mg/mL) was added dropwise to the zinc solution (50 mL, 10 mmol/L) $\text{Zn}(\text{CH}_3\text{COO})_2 \cdot 2\text{H}_2\text{O}$ (Sigma Aldrich, St. Louis, MO, USA) under stirring at 400 rpm. Then, 40 mg of $\text{Na}[\text{BH}_4]$ (Sigma Aldrich, St. Louis, MO, USA) as a reducing agent was added slowly to the mixture, and the final mixture was stirred for 24 h to allow reduction in GO into rGO and simultaneous formation of ZnO NPs [39]. Namely, at the same time GO and $\text{Zn}(\text{CH}_3\text{COO})_2 \cdot 2\text{H}_2\text{O}$ are reduced by $\text{Na}[\text{BH}_4]$ reducing agent. After reduction, remaining functional groups of rGO bound ZnO NPs. The final nanocomposite rGO-ZnO was washed three times with double-distilled water, while the final volume was adjusted to 10 mL. The rGO was prepared according to the same procedure but without adding $\text{Zn}(\text{CH}_3\text{COO})_2 \cdot 2\text{H}_2\text{O}$.

Working electrode preparation

A glassy carbon electrode (GCE) was polished on a pad with 1 μm and 0.3 μm alumina suspensions. Afterwards, it was subjected to sonication in double-distilled water–ethanol solution (50%, v/v) for 5 min, rinsed with water, and dried with filter paper. 10 μL of the prepared rGO-ZnO nanocomposite was subsequently pipetted dropwise on the GCE surface, and

dried by exposing to drier at 50 °C for 15 min. The proposed sensing platform was denoted as rGO-ZnO-GCE, and upon washing with water was ready for use. Furthermore, the same procedure was applied to fabricate the control electrodes such as ZnO-GCE and rGO-GCE. Then, the modified electrode was applied for the electrochemical determination of the TC.

Electrochemical measurements

The three-electrode system was immersed in an electrochemical cell containing 10 mL of the supporting electrolyte and an appropriate volume of TC standard solution. Cyclic voltammetry (CV) was utilized in order to investigate the redox behaviour and was performed in the potential range from + 0.5 V to + 1.2 V by applying step potential of 10 mV, scan rate range 10–500 mV/s, and equilibrium time of 5 s. The analytical performance and practical implementation were assessed using SWV, with prior optimization of instrumental parameters, and were performed in the anodic potential range from + 0.6 V to + 1.3 V.

To characterize and compare the electron transfer performance of modified and bare GCE electrodes, CV and electrochemical impedance spectroscopy (EIS) were used. Measurements were performed in 0.1 mol/L KCl aqueous solution containing 5 mmol/L $\text{K}_3[\text{Fe}(\text{CN})_6]/\text{K}_4[\text{Fe}(\text{CN})_6]$. CV was performed in the potential range from – 0.4 V to + 0.9 V under the scan rate of 0.05 V/s, while electrochemical impedance spectra were recorded in the frequency range from 0.1 to 10 kHz and with amplitude of 10 mV. The electrochemically active surface of modified rGO-ZnO-GCE or bare GCE was estimated from CV recordings, and the charge transfer properties of studied electrodes were evaluated by EIS.

Sample preparation

A sample of the tap water from laboratory was used. 2.00 mL of the tap water sample was transferred into the electrochemical cell containing 8.00 mL of the supporting electrolyte. The cell content was stirred for 10 s, and the SWV was performed. Since no detectable signals were obtained, the sample was spiked with TC standard solution (20 $\mu\text{mol/L}$).

A human urine sample was obtained from a healthy volunteer on the day of the experiment and

stored in the refrigerator until the moment of the analysis. 1.67 mL of the urine sample was transferred into the electrochemical cell filled with 8.33 mL of the supporting electrolyte, and after stirring the content was analysed by SWV. No detectable signals were obtained, and the solution in the cell was enriched with TC solution forming thus spiked human urine sample with TC concentration of 100 $\mu\text{mol/L}$.

Quantification of the antibiotic content in the spiked water and urine samples was performed by the standard addition method.

Scanning electron microscopy/energy-dispersive X-ray spectroscopy (SEM/EDS) analysis

The dispersion of the sample was applied on a silicon wafer from Siegert Wafer Company and allowed to dry at laboratory temperature (20–25 °C). This wafer was adhered by a carbon conductive tape to the stub that was inserted into the SEM MAIA 3 equipped with a FEG (field emission gun) from TESCAN Company (TESCAN Ltd. Brno, Czech Republic). The best photographs were obtained using the In-lens SE detector at a working distance between 4.89 and 5.02 mm and at 5 kV acceleration voltage. 768×858 pixel images were obtained at 50,000–100,000 fold magnification covering a sample area of 4.15–5.54 μm . Full frame capture was performed in UH Resolution mode and image shift correction was enabled, and it took about 0.5 min with the $\sim 0.32 \mu\text{s}$ /pixel dwell time. The spot size was set at 2.4 nm.

Elements analysis was performed on MIRA 2 SEM from TESCAN Company equipped with EDX detector X-MAX 50 (Oxford instruments plc, Abingdon, UK). EDX analysis was realized with the same condition as photographs (high vacuum). Only work distance was different (15 mm), the accelerating voltage was 15 kV and Everhart–Thornley scintillation detector was used. Input energy was set at about 20,000–21,000 cts, output energy was about 15,000–16,000 cts and dead time fluctuated between 19 and 20%. The time for analysis was 20 min. The spot size was 120 nm.

Transmission electron microscopy/energy-dispersive X-ray spectroscopy (TEM/EDS) analysis

The sample was studied by HRTEM FEI Talos F200X operated at 200 kV with a maximum beam current of

1.0 nA. The lower amount of beam current was chosen due to graphene oxide in the sample so that it is not damaged. The microscope is equipped with a Super-X EDS system with four Silicon drift detectors (SDDs) enabling element mapping. The sample was prepared on Au grid-coated holy carbon film. The measured SAED patterns were evaluated by the ProcessDiffraction.

Atomic force microscopy (AFM)

AFM imaging of nanostructured surface was carried out using the Bruker Dimension FastScan microscope (Bruker Nano Surfaces, Santa Barbara, CA, USA) operated in PFQNM mode. Triangular silicon nitride cantilever SCANASYST-AIR (Bruker AFM Probes, Camarillo, CA, USA) equipped with pyramidal silicon tip was used to characterize surface topography. Cantilever stiffness and sensitivity were calibrated by analysis of thermal noise spectra and were found to be 0.38 N/m and 78.5 nm/V, respectively. The following parameters were used to drive the AFM microscope: scanning speed 0.5 Hz, setpoint force value 1.25 nN, iGain value 0.75, number of points per line 1500. The raw recorded AFM data were processed in Bruker NanoScope Analysis ver. 2.0 (Bruker Nano Surfaces), where the 2D and 3D images of the surface were analysed and final figures were exported.

Fourier transforms infrared spectra (FTIR)

FTIR spectra were collected using an INVENIO® R FTIR Spectrometer equipped with a single-reflection diamond ATR accessory–A225/Q Platinum ATR module (Bruker Optic Inc., Billerica, MA, USA). Samples were freeze-dried using a Labconco Free-Zone® 2.5 Liter Freeze Dry System (Labconco; Kansas City, MO, USA). The fixed load was applied to the small amount of sample to ensure full contact of solid with the diamond ATR. Solid samples were directly analysed in lyophilized form. Before each measurement background spectra were collected. Spectra were recorded at 25 °C from 4000 to 400 cm^{-1} at a resolution of 2 cm^{-1} . Each spectrum was acquired by merging 128 interferograms. Bruker OPUS 8.1 (Bruker Optic Inc., Billerica, MA, USA) software was used for IR spectra recording and JDXview v0.2 software was used for further spectra evaluation.

Elemental analysis

All CHNS/O measurements were performed using FLASH 2000 (ThermoFisher Scientific Inc., Waltham, MA, USA) organic elemental analyser. The standards used for measurement were purchased from ThermoFisher Scientific Inc. For CHNS measurement 1–3 mg of measured sample was placed in a soft tin container and introduced into a quartz reactor filled with copper oxide and electrolytic copper. The reactor was heated to 950 °C and a small volume of oxygen was injected along with the sample. The gases released by the combustion of the sample were measured by the machine's in-built detector. The relative CHNS content was determined by comparing the resulting spectra to a BBOT (2,5-Bis(5-tert-butyl-2-benzo-oxazol-2-yl)) standard. For oxygen measurement the process was analogous. 1–2 mg of the sample was placed in a soft silver container and introduced to a quartz reactor filled with Nickel plated carbon and quartz turnings. The temperature of the reactor was 1080 °C. The oxygen percentage in the sample was determined via comparison to a spectrum of an acetanilide standard.

X-ray fluorescence

An elemental analyser SPECTRO XEPOS energy-dispersive X-ray fluorescence (ED-XRF) spectrometer (SPECTRO Analytical Instruments GmbH, Kleve, Germany) equipped with a 10 mm² Si-Drift Detector with Peltier cooling and a 7 µm Be side window was employed. The instrument uses a Pd-target end window tube at a maximum power of 50 W and a maximum voltage of 50 kV. Spectral resolution of the instrument (FWHM) is < 170 eV for Mn K α (measured under input count rate 10,000 pulses). SPECTRO XEPOS was operated and data were evaluated by means of the software Spectro X-Lab Pro, Version 2.5. For zinc determination Mo secondary target (tube voltage 44.70 kV, tube current 0.5 mA, measurement duration 1200 s, impulse rate 3,500–10,000 cps, relative dead time 2.3–5.7%, peak time 2.1 µs, gain 25.0 eV channel⁻¹, zero peak rate 5,000 cps, K α , Series Fit) was used. Solid sample (H₃BO₃ mixed with 5 mL of sample, dried, ground and pressed into a pellet) was measured directly in a sample cup (32 mm in diameter) on polypropylene X-Ray thin-film TF-240, 4 µm (FluXana, Bedburg-Hau, Germany) in a vacuum using the so-called Turboquant method

(fundamental parameters method). In order to determine the concentration of Zn a calibration curve was prepared (Fig. S1) using Zinc Standard for AAS (Sigma-Aldrich, 1000 mg/L). Precise amounts of the standard (3 mg, 7 mg, 14 mg and 21 mg) were pressed into H₃BO₃ pellets in triplicate. Utilizing the count rate of pulses at K α , Series Fit a calibration curve was created via linear regression.

Raman spectroscopy

Raman spectra were recorded on dispersive inVia Reflex Raman microscope (Renishaw, UK) with integrated Leica microscope DM2700 (Leica, Germany) and controlled by Wire 5.2 software (Renishaw, UK). Diode laser with an excitation wavelength of 633 nm and 17 mW power was used. Spectra were collected over the approximate range of 100–3200 cm⁻¹ using microscope immersion objective 50 × and a power setting of 100%. Each spectrum was acquired by merging 16 scans.

X-ray powder diffraction (XRPD)–samples preparation

A thin layer of a corresponding sample was deposited on a surface of a Si zero background sample holder (ZBH) by evaporating water from the suspension. All the as-prepared samples on ZBH were then placed into the sample holders for XRPD analysis.

X-ray powder diffraction—conventional Bragg–Brentano reflection geometry

Diffraction patterns were collected with the PANalytical X'Pert PRO diffractometer equipped with a conventional X-ray tube (Cu K radiation, 40 kV, 30 mA) and a linear position sensitive detector PIXcel with an anti-scatter shield. A programmable divergence slit set to a fixed value of 0.25 deg., Soller slit of 0.04 rad and mask of 15 mm were used in the primary beam. A programmable anti-scatter slit set to a fixed value of 0.25 deg., Soller slit of 0.04 rad and Ni beta-filter were used in the diffracted beam. Data were collected in the range of 5–90 deg. 2theta with the step of 0.0131 deg. and 500 s/step producing a scan of about 3 h 46 min.

Evaluation of X-ray patterns

Qualitative analysis was performed with the HighScorePlus software package (Malvern PANalytical, The Netherlands, version 4.9.0) together with the PDF-4 + database [40]. The line profile analysis was performed using routines implemented in the HighScorePlus software [41]. Diffraction lines were fitted using the Pseudo Voigt profile function with split width and shape. No background subtraction was performed. The calculated values of integral breadths of diffraction lines (Bobs) were then corrected for the instrumental broadening (Bstd). The net values of integral breadths (Bstruct) and the positions of diffraction lines were then entered into the Scherrer formula [42] to get the appropriate crystallite size in the corresponding direction. K (crystal shape factor) corresponding to a cubic shape of particles ($K = 1$) was used.

The correction for instrumental broadening was performed with the NIST SRM660a standard (LaB6) that was analysed with the same geometry and the Bstd values were determined by the same procedure.

X-ray photoelectron spectroscopy

The surface chemistry has been analysed by the XPS (X-ray photoelectron spectroscopy) technique. The high vacuum chamber was equipped with SPECS X-Ray XR50 source, where Al and Mg cathodes were used, and with a hemispherical analyser SPECS PHOIBOS 100 with 5-channels detector. The pressure before the measurement was about 3×10^{-9} mbar in the instrument. The elemental composition was calculated from area of selected high-resolution peaks taken at pass energy of 10 eV and using corresponding relative sensitivity factors used from Casa XPS library. The samples were inserted to a loading chamber in pot and dried directly there.

Results and discussion

Characterization of rGO-ZnO nanocomposite

The morphologies of GO as a starting material and rGO-ZnO were evaluated by SEM/EDS. The SEM image (Fig. 1a) confirmed the microstructure of the prepared GO by modified Hummers' method. GO

has a typical uniform smooth surface and large size of the sheet of GO. The size and morphology of ZnO NPs were confirmed (Fig. 1b). Figure 1c shows the SEM image of composite rGO-ZnO, where ZnO NPs (red arrow) can be observed on the surface of rGO (blue arrow). To observe separate ZnO NPs, TEM was used and in Fig. S2 uniform ZnO NPs which cover the surface of rGO can be seen.

SEM image of the site was subjected to elemental analysis (EDS). The elemental mapping (Fig. 2) confirmed the presence of zinc and oxygen, as well as carbon. Namely, the red colour indicates the carbon (C) that was measured for the K (alpha) 1 and 2 lines, the blue colour indicates the oxygen (O) that was measured for the K (alpha) 1 line, and the yellow indicates the zinc (Zn), which was measured for the L (alpha) 1 and line 2.

FTIR spectra were obtained for GO and composite rGO-ZnO (Fig. S4). The spectra show a broad peak ($2500\text{--}3700\text{ cm}^{-1}$) which corresponds to O–H groups in both analysed materials. Absorption peaks at 1646 and 1634 cm^{-1} belong to C=C groups. Vibrations at 1181, 1065, and 1041 cm^{-1} were assigned to C–O and from that 1065 and 1041 cm^{-1} belong to primary alcohols. The peak located at 1393 cm^{-1} represents the C–H group. The peak observed at 1506 cm^{-1} is due to aromatic C=C, which is common in this region. A large amount of remaining functional groups in rGO-ZnO suggest a mild reduction in the composite. The reductive capabilities of $\text{Na}[\text{BH}_4]$ are the most effective against carbonyl groups and low or moderate effective for carboxylic and epoxy groups [43].

AFM analysis was performed to investigate the topography and morphology of the rGO-ZnO. The height difference in three-dimensional topography was approximately 50 nm which confirms the size of particles onto rGO in the nanoscale (Fig. 3). AFM analysis also enables us to observe the uniform distribution of nanoparticles on the rGO surface.

By elemental analysis of rGO-ZnO nanocomposite, it was determined that the sample contained carbon and oxygen in large amounts probably because of the chemical composition of rGO which is constituted from carbon and remaining carbon-rich functional groups (Table 1, the results are displayed in the mass ratio w/w). A large amount of oxygen can be detected also because of the presence of ZnO NPs. An amount of hydrogen can be present because of hydroxyl, carbonyl, and carboxyl functional groups onto rGO.

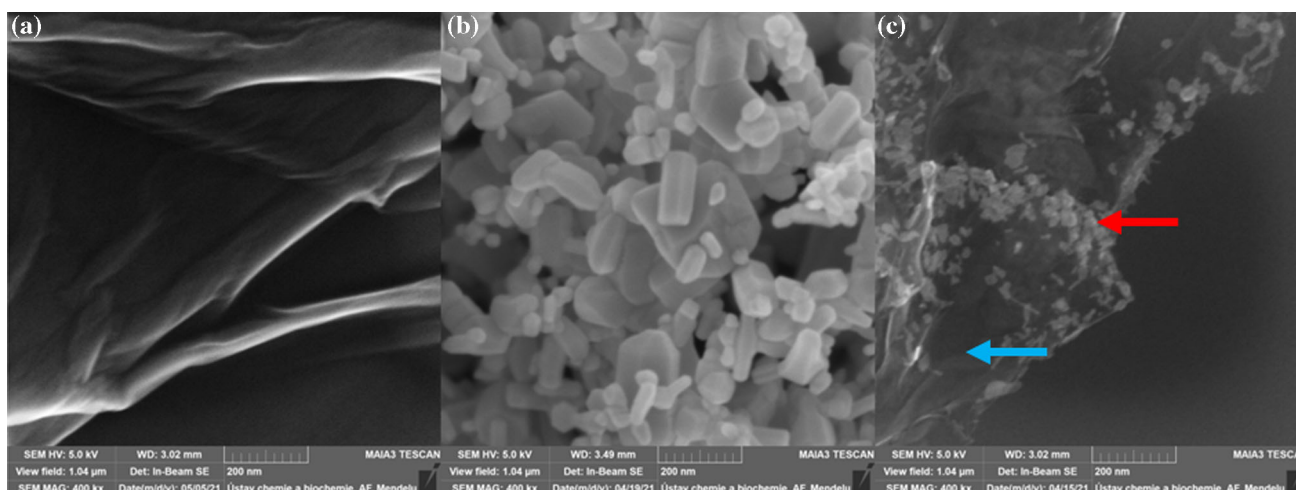


Figure 1 SEM images of **a** GO as an original material, **b** ZnO NPs and **c** nanocomposite rGO-ZnO.

The trace amount of nitrogen can be possibly present because of contamination during the sample preparation. The concentration of zinc was determined using X-ray fluorescence as 2.24 g/L.

The Raman spectroscopy of rGO-ZnO and GO was performed (Fig. 4). On the Raman spectrum of rGO-ZnO the intensity peaks at 1321 cm^{-1} and 1589 cm^{-1} correspond to the D and G bands, respectively. The G peak is responsible for the presence of sp^2 carbon, whereas the D peak refers to the presence of disorder in the graphene structure [44]. The presence of D and G peaks in the nanocomposites refers that the structure of rGO is preserved in the composites. The peaks at 427 cm^{-1} , 319 cm^{-1} , and 195 cm^{-1} in the composite are assigned to E2^{high} , $\text{E2}^{\text{high}}\text{-E2}^{\text{low}}$, and E2^{low} modes frequencies, respectively, and confirm the presence of ZnO in the composite [45, 46]. In the case of GO (Fig. 4), it is evident that GO has a higher D band in comparison to rGO-ZnO. This is due to the disruption of sp^2 bonds of the carbon because of GO's oxidative functional groups. Namely, if the D peak is higher, it means that the sp^2 bonds are broken and consequently there are more sp^3 bonds. The ratio of the intensity of D/G peaks relates to sp^3/sp^2 carbon ratio and measures the defects present on carbon nanomaterials structure. The I_D/I_G ratios of rGO-ZnO and GO were 0.96 and 1.17, respectively. It indicates the reduction in GO and recovery sp^2 bonded carbon atoms in the structure.

Figure 5 shows XRD patterns of rGO-ZnO and rGO. The characteristic diffraction lines of ZnO (PDF-4 + # 00-036-1451) were observed in the rGO-ZnO suggesting the successful formation of ZnO NPs.

Typical diffraction lines belonging to rGO are not clearly visible in rGO-ZnO. There are two explanations: 1) the intensities of lines belonging to ZnO are significantly higher and sharper than the semi-amorphous hill-like lines of the rGO; 2) Additionally, there are other NPs detected by TEM analysis that contain Zn, C and O (Fig. S3). These NPs are most probably hydrozincite (PDF-4 + # 04-013-7572). Therefore, two zinc-containing species exist in the composite material. Although zinc is a moderate absorber of X-rays, it absorbs significantly more than carbon. Moreover, hydrozincite and rGO are semi-amorphous. Therefore, it is very difficult to observe diffraction lines of rGO in that badly resolved system. The XRD patterns of rGO (Fig. 5) show the peak ($2\theta = 10.8^\circ$) of the large interlayer distance typical for GO because of the presence of a large number of functional groups in the structure of GO almost disappeared. The broad diffraction peak around ($2\theta = 25.7^\circ$) is recognizable for rGO, which indicates the highly amorphous nature of rGO and the results suggest that GO has been reduced to rGO using NaBH_4 [47, 48].

The XPS survey spectra of the rGO-ZnO sample (Fig. 6) show the presence of the expected element C, O and Zn. The only detected impurity on the surface is Na. The comparison of the spectra recorded with different wavelengths shows a high number of Auger peaks not present in the CasaXPS library.

The surface composition calculated from the high-resolution spectra C 1s, O 1s and Zn 2p shows the following concentrations 35.5 at. %, 40.0 at. %, and 24.5 at. %, respectively. The high content of the

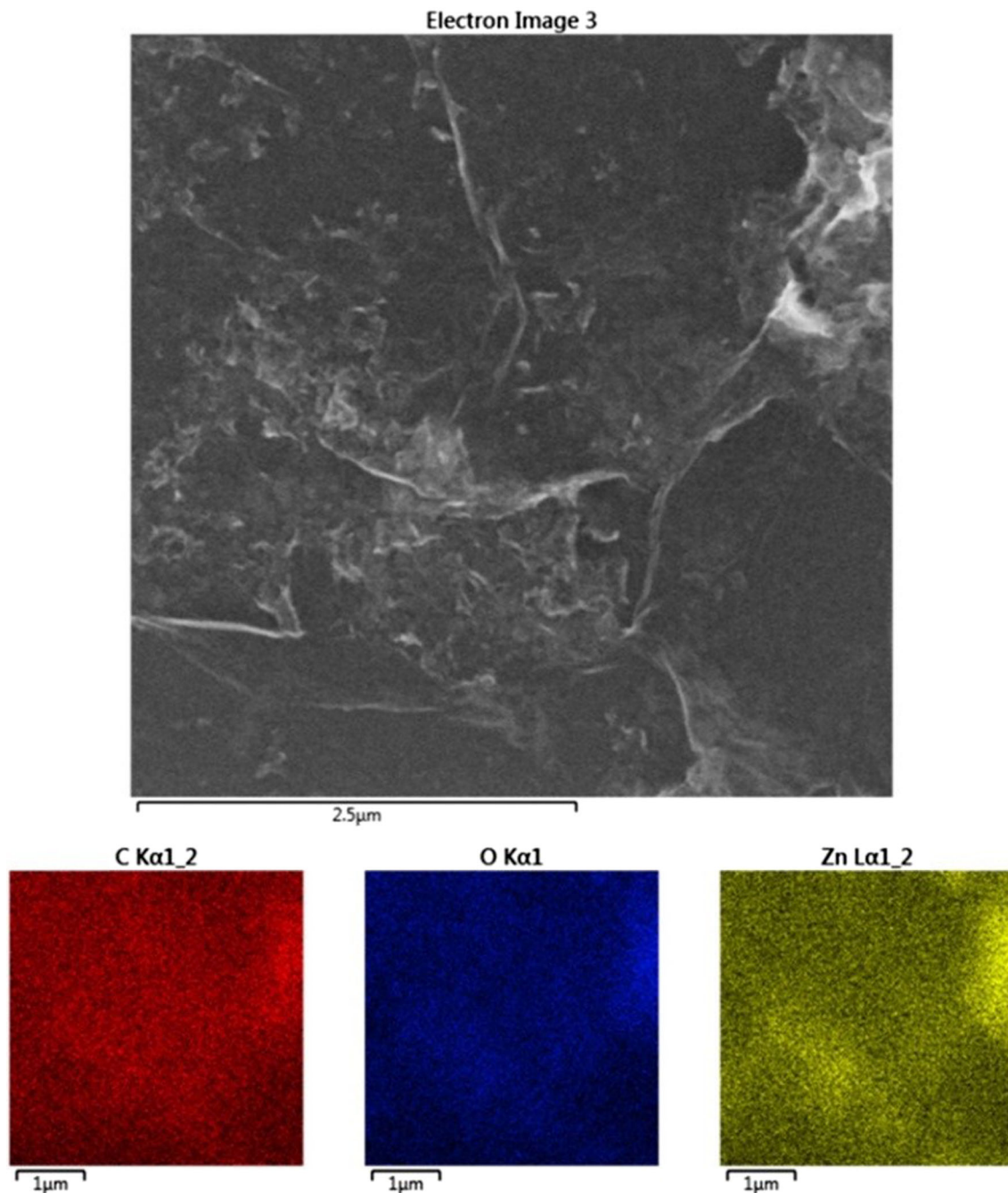


Figure 2 SEM–EDS elemental mapping of rGO-ZnO composite.

oxygen indicated the presence of O–C bonds in GO and ZnO NP. To prove this claim, C 1s peak was deconvoluted in the individual components related to sp² at 284.5 eV, sp³ at 285.1 eV, C–O at 287.0 eV, and C=O–OH at 290.3 eV [49, 50]. The presence of sp² and sp³ bonds is confirmed also in Raman spectra, the ratio sp²/sp³ measured by XPS shows a bit value therefore is probable the sp³ states are

presented more on the surface, therefore, promoted in XPS spectra compared to Raman spectra. The relative number of carbon atoms bonded to oxygen is about 83% of what is expected for GO and it explains the high amount of oxygen present in rGO-ZnO sample. The zinc-related peak Zn 2p is known to be less sensitive towards chemical changes. However, the detailed study of the Zn 2p_{3/2} peak related to NP

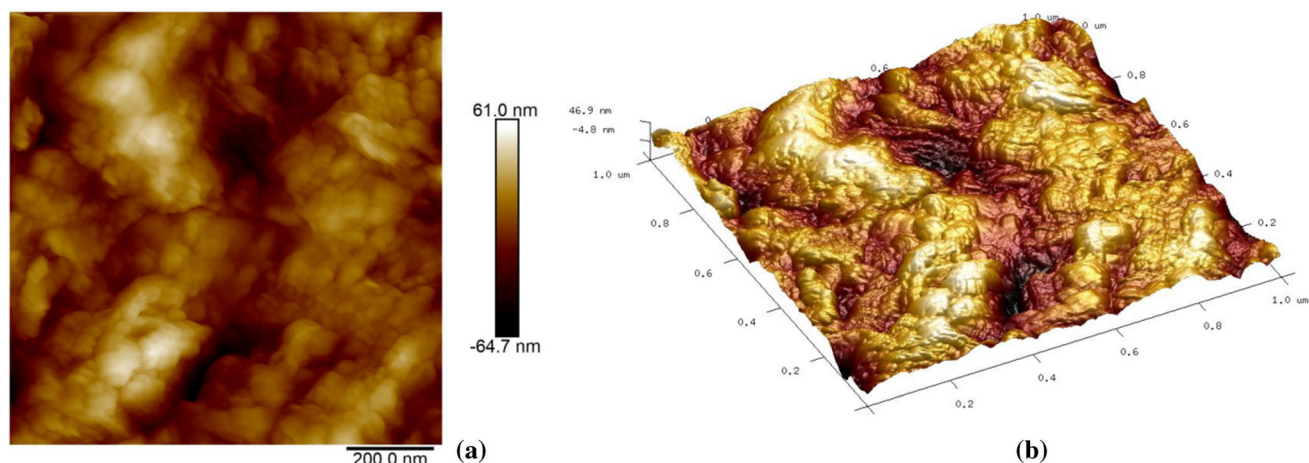


Figure 3 2D **a** and 3D **b** AFM image of nanocomposite rGO-ZnO.

Table 1 Elemental analysis (C, H, N, O, S) of nanocomposite rGO-ZnO

| Nitrogen (%) | Carbon (%) | Hydrogen (%) | Sulphur (%) | Oxygen (%) |
|-----------------|------------------|-----------------|-----------------|------------------|
| 0.21 ± 0.06 | 13.09 ± 0.74 | 1.00 ± 0.07 | 0.00 ± 0.00 | 37.75 ± 0.60 |

The results are displayed in the mass ratio (w/w)

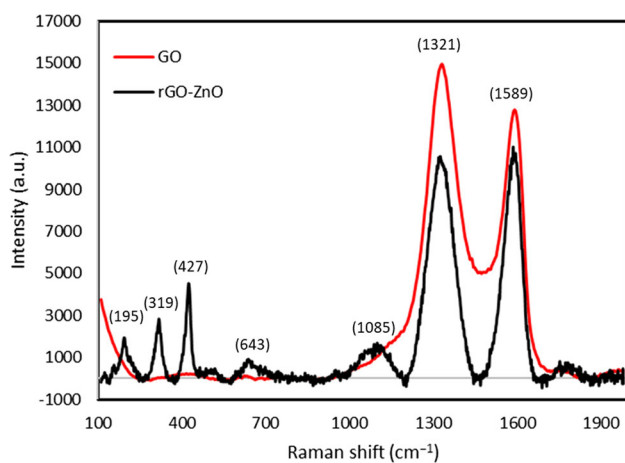


Figure 4 Raman spectra of rGO-ZnO (black line) and GO (red line).

in literature [51] suggests that the observed single peak character of Zn 2p_{3/2} is ZnO with a size above 10 nm. It is in agreement with SEM observation and sharp XRD peaks. The chemical bonding state of Zn can be also studied with the use of the Auger parameter. The Auger parameter is about 2010 eV which can be ZnO [52]. The oxygen-related peak O 1s shows two main components related to O-C in GO at 533.3 eV and O-Zn at 532.0 eV [53]. Therefore, we can confirm the presence of ZnO with GO in the analysed material where both sp² and sp³ states are present.

Electrochemical sensing characterization of modified electrodes

The electrochemical properties of the rGO-ZnO-GCE were investigated with the use of CV and EIS (Fig. 7), and the measurements were performed in a 0.1 mol/L KCl aqueous solution containing 5 mmol/L K₃[Fe(CN)₆]/K₄[Fe(CN)₆]. For comparison purposes, parallel experiments with bare GCE were done as well. CV is a useful tool to acquire information regarding electrochemical performance of the modified electrodes. The results of CVs experiments with bare GCE and rGO-ZnO-GCE are shown in Fig. 7a. As shown in Fig. 7a, modification of the GCE surface by rGO-ZnO leads to an increase in both anodic (I_{Pa}) and cathodic (I_{Pc}) peaks currents, due to the activity of nanocomposite. ΔE_p values were more than the theoretical of 59 mV and the ratios of I_{Pa}/I_{Pc} were close to 1 for all the electrodes, demonstrating quasi-reversible processes [54]. By using the Randles-Sevcik equation [55] the active surface area of the rGO-ZnO-GCE working electrode available for the electron transfer to species in the solution was calculated to be 0.0493 cm², which is 1.5 larger than that of GCE (0.0329 cm²). Those results confirmed that rGO-ZnO nanocomposite improves the electroactive surface area greatly, and eventually causes the significant

Figure 5 X-ray diffraction of rGO-ZnO (black line) and rGO (grey line).

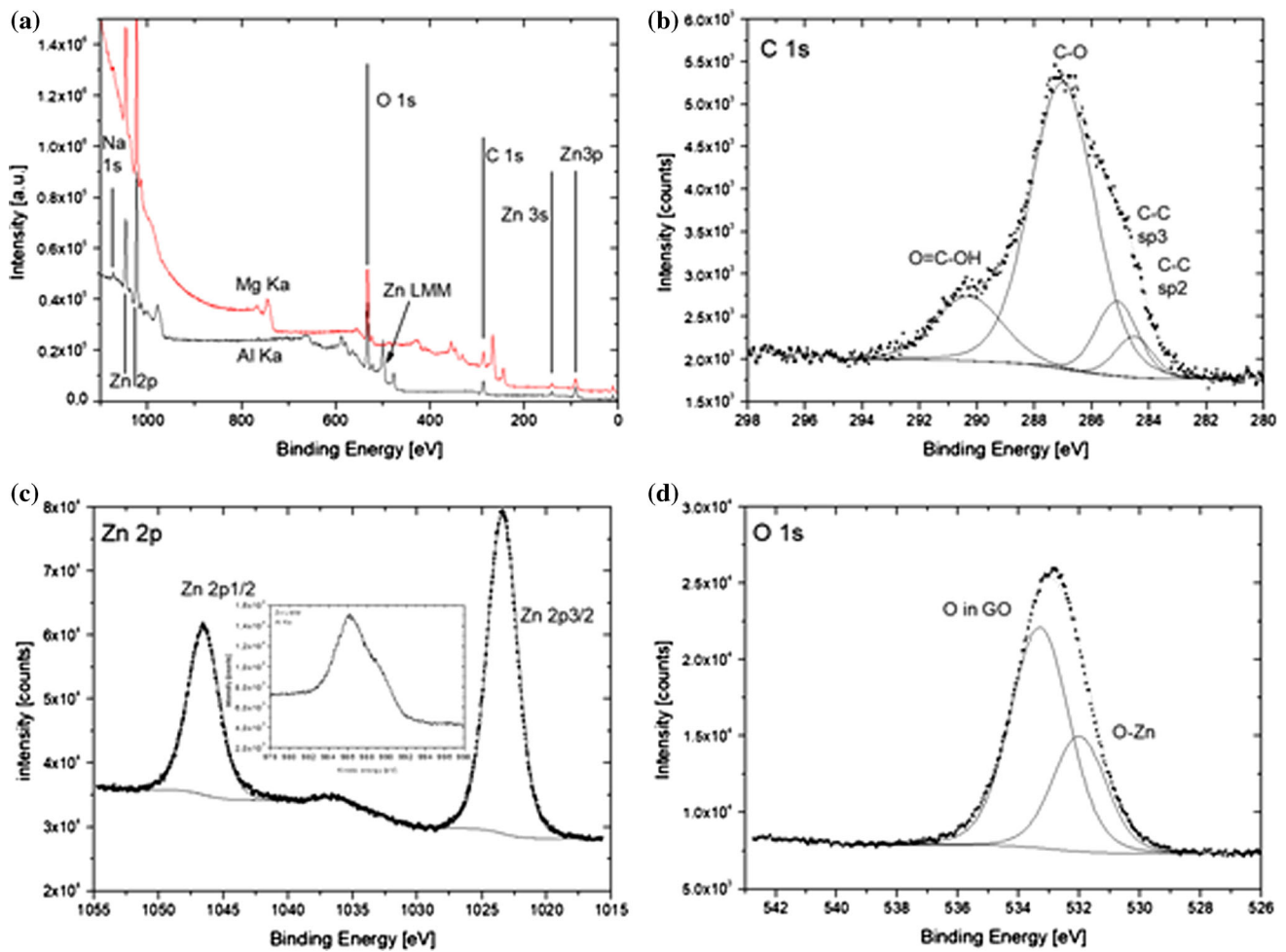
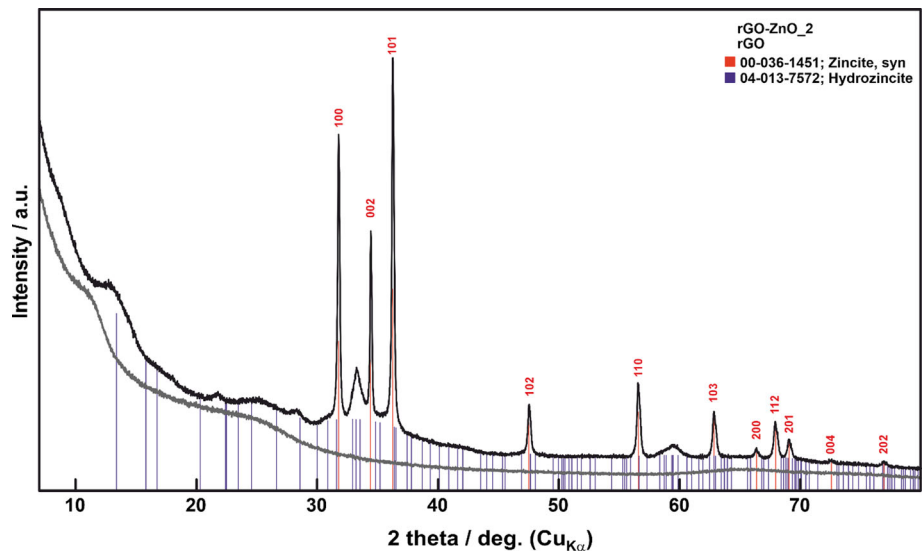


Figure 6 XPS spectra of rGO-ZnO a survey spectra, high-resolution spectra of b C 1s, c Zn 2p with Zn LMM inset and d O 1s.

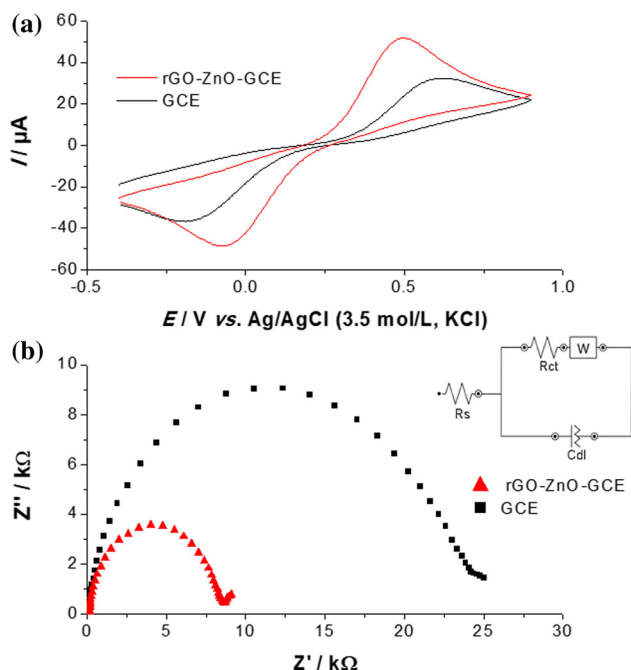


Figure 7 **a** CV responses of GCE and rGO-ZnO-GCE in 5 mmol/L $\text{Fe}(\text{CN})_6^{3-}/\text{Fe}(\text{CN})_6^{4-}$ in 0.1 mol/L KCl; **b** EIS response of GCE and rGO-ZnO-GCE in 5 mmol/L $\text{Fe}(\text{CN})_6^{3-}/\text{Fe}(\text{CN})_6^{4-}$ in 0.1 mol/L KCl. Inset of **b**: the applied equivalent circuit.

increase in peak current response and sensitivity of the produced sensor.

To obtain precious information about the kinetics of electron transfer at the electrode surface, a powerful EIS technique was used. The electrochemical impedance spectra of bare GCE and rGO-ZnO-GCE are shown in Fig. 7b in the form of the Nyquist diagrams. The Randles circuit (inset of Fig. 7b) was applied for data fitting. The diameter of the semicircle of the Nyquist plot is an indication of the charge transfer resistance (R_{ct}) at the electrode–solution interface [55]. It is evident from Fig. 7b that the semicircular diameter of the rGO-ZnO-GCE is smaller in comparison to GCE, which suggests that rGO-ZnO nanocomposite curtailed electron transfer resistance, respectively, increased the electrical conductivity and facilitated electron transfer. Additionally, the obtained fitting results for the R_{ct} value were 19.00 $\text{k}\Omega$ and 7.16 $\text{k}\Omega$ for bare GCE and rGO-ZnO-GCE, respectively. Those results reflect the conclusions obtained from the CV experiments. Altogether, the presence of rGO-ZnO nanocomposite promoted the electron transfer rate significantly and consequently contributed to the improved conductivity

and larger specific surface area of the electrode. Therefore, rGO-ZnO can be used to fabricate electrochemical sensors.

Electrochemical behaviour of TC

Reduced graphene oxide with 2D structure, large theoretic surface area, chemical stability, and high electrical conductivity is suitable material for electrochemical applications [56]. Zinc oxide exhibits optic, sensing, catalytic, and semiconducting properties [34–37]. In recent years, the development and interest of composite nanomaterials from carbonaceous nanostructures and metal oxides for electrochemical applications have risen [57].

The preliminary study was aimed towards comparing the voltammetric behaviour of TC using bare GCE and modified ZnO-GCE, rGO-GCE and rGO-ZnO-GCE. The experiments were performed in 0.1 mol/L BRB pH 8.0 using a SWV as a suitable voltammetric technique which is more sensitive than a CV. The electrochemical responses of 200 $\mu\text{mol/L}$ TC using those four comparable working electrodes by performing SWV are shown in Fig. 8. At the bare GCE, the oxidation peak corresponding to TC was relatively broad and weak ($I_{P(\text{GCE})} = 0.575 \mu\text{A}$). The TC oxidation current on rGO-GCE ($I_{P(\text{rGO-GCE})} = 1.115 \mu\text{A}$) was enhanced in comparison to that on GCE. The peak current height of TC on ZnO-GCE was magnified additionally ($I_{P(\text{ZnO-GCE})}$

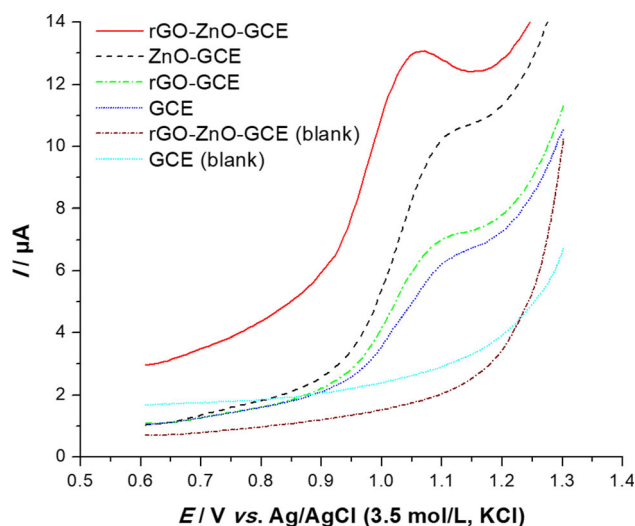


Figure 8 Square-wave voltammograms of 200 $\mu\text{mol/L}$ TC in 0.1 mol/L BRB pH 8.0 at bare GCE, rGO-GCE, ZnO-GCE and rGO-ZnO-GCE.

$GCE) = 2.063 \mu A$). However, the sharpest voltammetric peak and at least six times higher current response ($I_{P(rGO-ZnO-GCE)} = 3.452 \mu A$) were obtained at rGO-ZnO-GCE. Moreover, the oxidation potential of TC at rGO-ZnO-GCE (+ 1.04 V) shifted slightly at the cathodic range when compared to the signals obtained at ZnO-GCE (+ 1.08 V), rGO-GCE (+ 1.09 V) and GCE (+ 1.10). The enhancement of the peak current response may be owed to the synergistic effect of rGO and ZnO [33, 37]. Namely, the rGO provides a large electrochemical active surface and good conductivity [28], while ZnO has potent electrocatalytic performance [35]. Consequently, the use of rGO-ZnO-GCE as a sensitive electrochemical sensing platform for TC detection in this study was reasonable.

Influence of the supporting electrolyte and pH on the electrochemical detection of TC

To obtain the maximum sensitivity of rGO-ZnO-GCE towards TC determination, as the initial experimental parameter, which mostly influences the analytical performance of the proposed electrochemical sensor, was considered to be the composition of the supporting electrolyte, its concentration and pH value. The effect of the supporting electrolyte on the electrochemical response of the rGO-ZnO-GCE was studied in several buffer solutions, including BRB, acetate, citrate and phosphate buffer. For that purpose CV and SWV were performed in the solution containing increasing concentration of the analyte (5–50 $\mu\text{mol/L}$) and the potential was scanned in the anodic direction from + 0.60 V to + 1.20 V. Apparently, the BRB was the most favourable for TC oxidation under the tested conditions (Fig. S5) and thus it was adopted as an optimal buffer for further experimental study.

The concentration of BRB influences the voltammetric determination of TC. Consequently, the effect of BRB concentration (0.02; 0.04; 0.08; 0.10 and 0.20 mol/L) on TC analytical signal was studied in the solution containing 50 $\mu\text{mol/L}$ TC (Fig. S6a). The best results in terms of signal sharpness and height were obtained in 0.10 mol/L BRB, which was acquired as optimal in further experiments.

In order to explore the optimal pH for the development of analytical procedure in further experiments, voltammograms of TC (20 and 50 $\mu\text{mol/L}$ TC)

were recorded in 0.10 mol/L BRB supporting electrolyte with different pH values from 2.0 to 10.0 (Fig. S6b). Due to the best-shaped peak and the highest peak current, the supporting electrolyte of pH value 8.0 was chosen for further examination.

By analysing the dependence of the anodic peak potential on pH, slight displacements in the peak potential to less positive values were observed in the pH range from 2.0 to 6.0. The linear regression equation was obtained with a slope of 0.048 V/pH, which is close to the theoretical Nernst value (0.059 V/pH), indicating that an equal number of protons and electrons ($2H^+/2e^-$) are involved in the electrochemical oxidation. However, no significant change in the peak potential was observed with pH between 7.0 and 10.0. Similar behaviour of some TCs was found by other authors in the literature [24, 26]. From those results, the electrochemical oxidation of TC on rGO-ZnO-GCE is anticipated to be complicated. Considering our results and the previously published data, it can be assumed that the phenolic moiety in position 10 and/or a dimethylamino substituent on position 4 are likely sites for electrochemical oxidation [19, 24, 26, 58].

Electrochemical behaviour

To obtain additional information regarding the electrochemical behaviour of TC on rGO-ZnO-GCE, CV using different scan rates was performed. The measurements were carried out in 0.1 mol/L BRB pH 8.0, as an optimal supporting electrolyte, containing 200 $\mu\text{mol/L}$ of TC (Fig. S7). The results showed that one oxidation peak at the potential of + 1.07 V was observed, while the absence of the reduction peak in the reverse scan indicates the irreversibility of the electrode reaction. The effect of the scan rate (ν) on the anodic peak current (I_p) was tested in the scan rate range from 10 to 500 mV/s. The results of this study showed that TC oxidation peak current increases with an increase in the scan rate, while the linear relationship between I_p and the square root of the scan rate ($\nu^{1/2}$) was obtained ($R^2 = 0.9985$, inset (a) of Fig. S7). This signifies that the reaction which takes place on the working electrode is a diffusion-controlled process. A slope value obtained by plotting the logarithm of peak current ($\log I_p$) vs. the logarithm of the scan rate ($\log \nu$) is equal to 0.502 ($R^2 = 0.9993$, inset (b) on Fig. S7), confirming thus the

diffusion-controlled process on the working electrode.

Optimization of the voltammetric parameters

The optimization of the most important SWV parameters which affect the determination of TC using rGO-ZnO-GCE was studied, including modulation amplitude (E_{sw}), step potential (ΔE), frequency (f) and equilibrium time (t_{eq}) (Fig. S8). Experiments were performed in BRB (0.1 mol/L, pH 8.0) containing 50 $\mu\text{mol/L}$ TC in a potential range from + 0.6 to + 1.3 V. During optimization, each parameter was gradually changed, while others were kept at a constant value. The relation between peak current and amplitude was studied in the range 10–200 mV. The peak current increased with increasing the E_{sw} value and reached a maximum value of 0.70 μA at E_{sw} value of 50 mV, with subsequent stagnation in the interval from 50 to 100 mV, and a sudden decrease in peak current value at amplitude values higher than 100 mV (Fig. S8a). The influence of the frequency was investigated in the range of 10–100 Hz. With increasing frequency value, an increase in the height of the analytical signal was observed (Fig. S8b), but in the choice of the optimal value of this parameter, the decisive factor was the appearance of the analytical signal. In further work, the optimal value of the frequency of 50 Hz was adopted, at which the best shape of the analytical signal is achieved, and no distortion of the peak is noticeable. In the next step, the value of ΔE was changed in the interval 1–20 mV. In that range there was an increase in the peak current up to 7.5 mV, in the range of 7.5–15 mV the peak current did not change significantly, with a subsequent sharp drop in its value (Fig. S8c). The last tested parameter— t_{eq} , was changed from 0 to 30 s. Up to 10 s there was no significant change in the signal height, while with a subsequent increase, the peak current sharply decreased (Fig. S8d). By summarizing the optimization results, it appeared that the sensor showed the best performance at the following SWV instrumental parameters: E_{sw} of 50 mV, f of 50 Hz, ΔE of 7.5 mV and t_{eq} of 10 s.

Analytical features

The voltammetric profiles of different concentrations of TC were recorded in order to define the linearity

range of the proposed method. The calibration curve was constructed by plotting peak current responses (I_p) versus the concentration of TC (C_{TC}), and the linear regression equation was calculated by the least-squares method. Figure 9 shows the respective SW voltammograms using different TC concentrations with corresponding calibration curve (Inset of Fig. 9). The obtained calibration curve was linear over a wide concentration range from 4 to 400 $\mu\text{mol/L}$, with a correlation coefficient (R^2) of 0.9910. The analytical performance evaluation of the proposed methodologies is comprehensively summarized in Table 2. The limit of detection (LOD) and limit of quantification (LOQ) were calculated as: $\text{LOD} = 3.3 \sigma/S$, and $\text{LOQ} = 10 \sigma/S$, where σ stands for the standard deviation of the intercept, and S is the slope of the calibration curve [59]. For the proposed method LOD and LOQ were 0.38 $\mu\text{mol/L}$ and 1.15 $\mu\text{mol/L}$, respectively.

A comparison of the analytical parameters of the proposed and other sensors employed for TC quantification in real samples is summarized in Table 3. The results demonstrated that herein presented methodologies in a combination of rGO-ZnO-GCE as a sensor offers enviable sensitivity and application ability in a wider concentration range, compared to recently published electroanalytical methodologies.

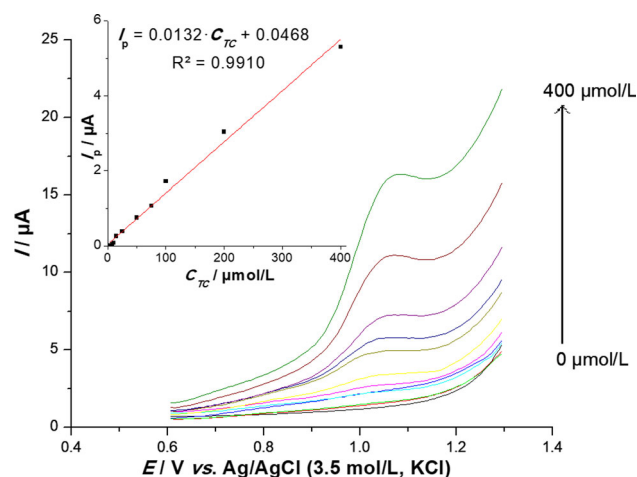


Figure 9 Square-wave voltammograms of TC (0, 4, 5, 7.5, 10, 15, 25, 50, 75, 100, 200 and 400 $\mu\text{mol/L}$) in 0.1 mol/L BRB, pH 8.0, using rGO-ZnO-GCE. Inset: Corresponding calibration curve (mean \pm 2SD, $n = 5$).

Precision

The precision of the proposed SWV method (intra- and inter-day) was evaluated by performing five repetitive analyses of TC (50 $\mu\text{mol/L}$) freshly prepared solutions on the same day, and five consecutive days by using developed SWV methodology. The relative standard deviation (RSD) values obtained in this study were lower than 3.40% (Table 2), indicating the high precision of TC assays by using the proposed electrochemical sensor. The reproducibility study was done by recording SWVs in the solution containing 50 $\mu\text{mol/L}$ of TC using five different rGO-ZnO-GCEs prepared in the same way. The observed RSD value for peak currents was 4.22%, indicating

that the preparation of the modified electrode was quite reproducible.

Interference study

In order to study the selectivity of rGO-ZnO-GCE prior to the application on real samples analysis, the electrochemical measurements were performed in the presence of some common accompanying substances. The maximum concentration of the potential interfering agent which causes a relative error of less than 5% for the peak current of TC (20 and 50 $\mu\text{mol/L}$) was considered as the tolerance limit. The results revealed that a 1000-fold excess of Na^+ , H_2PO_4^- , SO_4^{2-} , urea, a 500-fold of Ca^{2+} , a 100-fold excess of Cl^- , K^+ , and a 10-fold of NH_4^+ did not interfere with the determination of TC (Fig. S9). These results indicated that the proposed sensor possesses good selectivity towards the determination of TC even in the presence of potential interferences.

Table 2 The analytical performance of the developed methods using the SWV optimized procedure on rGO-ZnO-GCE

| Analytical performance evaluation | SWV |
|--|--------|
| Peak potential (V vs. Ag/AgCl, KCl 3.5 mol/L) | 1.05 |
| Linear concentration range ($\mu\text{mol/L}$) | 4–400 |
| Slope ($\mu\text{A}/\mu\text{mol L}$) | 0.0132 |
| Intercept (μA) | 0.0468 |
| Correlation coefficient (R^2) | 0.9910 |
| Limit of detection ($\mu\text{mol/L}$) | 0.38 |
| Limit of quantification ($\mu\text{mol/L}$) | 1.15 |
| Intra-day precision ($n = 5$), RSD (%) | 1.36 |
| Inter-day precision ($n = 5$), RSD (%) | 3.31 |

Analytical application

Practical application testing of the proposed method with rGO-ZnO-GCE for the determination of TC was done in water and human urine samples. The samples were diluted, injected into the electrochemical cell, and analysed directly using an optimized SWV procedure. No detectable signals were obtained during voltammetric analysis of diluted real samples. Spiked samples were analysed using the standard

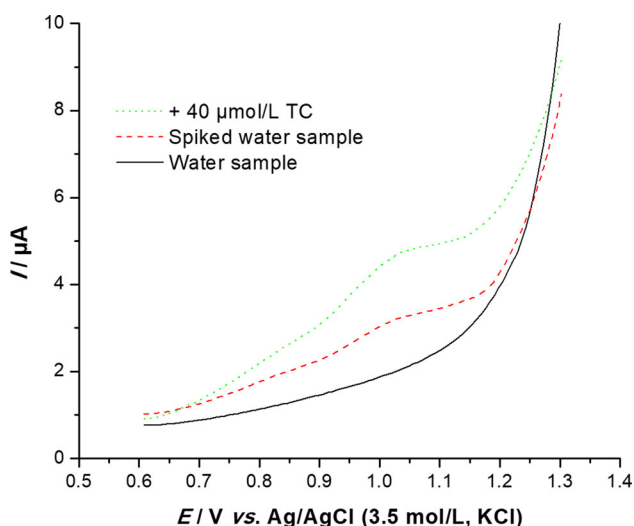
Table 3 Comparison of some validation parameters of the developed and previously reported electrochemical methods for TC determination

| Electrode | Technique | LOD ($\mu\text{mol/L}$) | Linear range ($\mu\text{mol/L}$) | Practical application | Reference |
|-------------------|-------------|---------------------------|------------------------------------|---|------------|
| BiFE | Amperometry | 1.2 | 500–6000 | Pharmaceutical | [18] |
| G-PCE | DPV | 2.3 | 3.8–19 | Human urine | [19] |
| GPU | DPV | 2.80 | 4–40 | Water | [20] |
| Pb-PFGE | Ads-DPCSV | 0.004 | 0.05–10 | Meat, milk, liver, honey | [21] |
| IL-MWCNT-GCE | LSV | 0.03 | 0.11–22 | Egg, Pharmaceutical | [22] |
| p-Mel@ERGO/GC | DPV | 5 | 10–80 | Human urine | [23] |
| PtNPs/C/GCE | DPV | 4.28 | 9.99–44.01 | Human urine | [24] |
| MWCNT-COOH-GO/CPE | AdSDPV | 0.36 | 20–310 | Water, artificial urine, pharmaceutical | [25] |
| rGO-ZnO-GCE | SWV | 0.38 | 4–400 | Water, human urine | This study |

BiFE, Bismuth film electrode; G-PCE, Graphite-polyurethane composite electrode; GPU, graphite-polyurethane composite electrode; Pb-PFGE, Pb-polyaminophenol filmed GCE; IL-MWCNT-GCE, Ionic liquid multi-walled carbon nanotube film-coated GCE; p-Mel@ERGO/GC, Polymelamine film electrochemically reduced graphene oxide GCE; PtNPs/C/GCE, platinum nanoparticles supported on carbon-coated GCE; MWCNT-COOH-GO/CPE, Carbon nanotubes with carboxyl groups graphene oxide modified CPE; rGO-ZnO-GCE, Reduced graphene oxide Zn oxide nanocomposite modified GCE

Table 4 The results obtained from the analysis of tap water and human urine sample using proposed SWV with rGO-ZnO-GCE

| Sample | Added ($\mu\text{mol/L}$) | Found ($\mu\text{mol/L}$) ^a | Recovery (%) |
|--------|-----------------------------|--|--------------|
| Water | 0 | n.d. ^b | – |
| | 20 | 19.53 \pm 1.66 | 97.64 |
| Urine | 0 | n.d. | – |
| | 100 | 97.63 \pm 1.84 | 97.63 |

^aMean \pm 2SD, $n = 3$ ^bNot detected**Figure 10** Analysis of tap water and spiked tap water samples by the standard addition method with the optimized SWV using rGO-ZnO-GCE.

addition method. The average results of three replicate measurements are presented in Table 4. Good recovery values, accompanied by low values of RSD of less than 4.3%, indicate that the proposed method is highly accurate, reproducible and precise. As an illustrative example of successfully performed voltammetric analysis in real samples, the particular SW voltammograms obtained in spiked water (20 $\mu\text{mol/L}$) and after the standard addition are presented in Fig. 10. It is evident that the SWV methodology using rGO-ZnO-GCE as an electrochemical sensing platform did not suffer from any considerable matrix effect. This fact enables the application of herein presented cheap and easily produced sensor for routine TC analyses in the analysis of environmental and clinical samples.

Conclusions

In this work, rGO-ZnO was prepared and used as a modifier of the GCE surface providing an electrochemical sensor for the determination of TC. The electrochemical behaviour of TC on rGO-ZnO-GCE was investigated by CV and SWV techniques. In comparison to GCE, the rGO-ZnO-GCE showed remarkable enhancement of the electrooxidation of TC. The rGO-ZnO-GCE sensor exhibits a relatively wide linear range and a low limit of detection. High sensitivity, excellent reproducibility and satisfy selectivity confirmed advantages of the proposed sensor, while a successful application in real sample analysis with accurate results validated the practical applicability of the proposed method. Since sensor is based on nanocomposite, the proposed method can be easily transferred to screen printed electrodes in order to be integrated into portable systems and can be used as disposable sensors for routine analysis in laboratory practice.

Acknowledgements

This work was supported by European Regional Development Fund “Multidisciplinary research to increase application potential of nanomaterials in agricultural practice” (No. CZ.02.1.01/0.0/0.0/16_025/0007314) and by the Ministry of Education, Youth and Sports of the Czech Republic under the Central European Institute of Technology (CEITEC) 2020 project (LQ1601). We acknowledged the Nanobiotechnology core facility supported by the Ministry of Education, Youth and Sports of the Czech Republic (LM2018127). Authors from the Faculty of Technology, University of Novi Sad acknowledge support from the Ministry of Education, Science and Technological development, Republic of Serbia (Project No. 451–03-68/2022–14/200134). The authors also acknowledge the assistance provided by the Research Infrastructure NanoEnviCz, supported by the Ministry of Education, Youth and Sports of the Czech Republic under Project No. LM2018124.

Declarations

Conflict of interest The authors declare that they have no conflict of interest.

Supplementary Information: The online version contains supplementary material available at <http://doi.org/10.1007/s10853-022-06926-1>.

References

- [1] Chopra I, Roberts M (2001) Tetracycline Antibiotics: Mode of Action, Applications, Molecular Biology, and Epidemiology of Bacterial Resistance. *Microbiol Mol Biol Rev* 65:232–260. <https://doi.org/10.1128/membr.65.2.232-260.2001>
- [2] Roberts MC (2003) Tetracycline therapy: Update. *Clin Infect Dis* 36:462–467
- [3] Nelson ML (2001) The chemistry and cellular biology of the tetracyclines. In: Nelson M, Greenwald W, Hillen RA (eds) *Tetracyclines in Biology, Chemistry and Medicine*. Birkhäuser, Basel, pp 3–63
- [4] Granados-Chinchilla F, Rodríguez C (2017) Tetracyclines in Food and Feedingstuffs: From Regulation to Analytical Methods, Bacterial Resistance, and Environmental and Health Implications. *J Anal Methods Chem Article ID*. <https://doi.org/10.1155/2017/1315497>
- [5] Baietto L, Corcione S, Pacini G, Perri GD, D'Avolio A, De Rosa FG (2014) A 30-years Review on Pharmacokinetics of Antibiotics: Is the Right Time for Pharmacogenetics? *Curr Drug Metab* 15:581–598
- [6] Bound JP, Voulvoulis N (2004) Pharmaceuticals in the aquatic environment - A comparison of risk assessment strategies. *Chemosphere* 56:1143–1155. <https://doi.org/10.1016/j.chemosphere.2004.05.010>
- [7] Aalipour F, Mirlohi M, Jalali M, Azadbakht L (2015) Dietary exposure to tetracycline residues through milk consumption in Iran. *J Environ Heal Sci Eng* 13:1–7. <https://doi.org/10.1186/s40201-015-0235-6>
- [8] Borghi AA, Palma MSA (2014) Tetracycline: Production, waste treatment and environmental impact assessment. *Brazilian J Pharm Sci* 50:25–40. <https://doi.org/10.1590/S1984-82502011000100003>
- [9] Zhao Y, Geng J, Wang X et al (2011) Tetracycline adsorption on kaolinite: PH, metal cations and humic acid effects. *Ecotoxicology* 20:1141–1147. <https://doi.org/10.1007/s10646-011-0665-6>
- [10] Pérez-Rodríguez M, Pellerano RG, Pezza L, Pezza HR (2018) An overview of the main foodstuff sample preparation technologies for tetracycline residue determination. *Talanta* 182:1–21. <https://doi.org/10.1016/j.talanta.2018.01.058>
- [11] Al-Afy N, Sereshti H, Hijazi A, Rashidi Nodeh H (2018) Determination of three tetracyclines in bovine milk using magnetic solid phase extraction in tandem with dispersive liquid-liquid microextraction coupled with HPLC. *J Chromatogr B Anal Technol Biomed Life Sci* 1092:480–488. <https://doi.org/10.1016/j.jchromb.2018.06.049>
- [12] Cherkashina K, Vakh C, Lebedinets S et al (2018) An automated salting-out assisted liquid-liquid microextraction approach using 1-octylamine: On-line separation of tetracycline in urine samples followed by HPLC-UV determination. *Talanta* 184:122–127. <https://doi.org/10.1016/j.talanta.2018.02.112>
- [13] Phiroonsoontorn N, Sansuk S, Santaladchaiyakit Y, Srijaranai S (2017) The use of dissolvable layered double hydroxide components in an in situ solid-phase extraction for chromatographic determination of tetracyclines in water and milk samples. *J Chromatogr A* 1519:38–44. <https://doi.org/10.1016/j.chroma.2017.09.005>
- [14] Chico J, Meca S, Companyó R et al (2008) Restricted access materials for sample clean-up in the analysis of trace levels of tetracyclines by liquid chromatography. Application to food and environmental analysis. *J Chromatogr A* 1181:1–8. <https://doi.org/10.1016/j.chroma.2007.12.033>
- [15] Koesukwiwat U, Jayanta S, Leepipatpiboon N (2007) Validation of a liquid chromatography-mass spectrometry multi-residue method for the simultaneous determination of sulfonamides, tetracyclines, and pyrimethamine in milk. *J Chromatogr A* 1140:147–156. <https://doi.org/10.1016/j.chroma.2006.11.099>
- [16] Ibarra IS, Rodriguez JA, Miranda JM et al (2011) Magnetic solid phase extraction based on phenyl silica adsorbent for the determination of tetracyclines in milk samples by capillary electrophoresis. *J Chromatogr A* 1218:2196–2202. <https://doi.org/10.1016/j.chroma.2011.02.046>
- [17] Gao F, Zhao GX, Zhang HC et al (2013) Production of monoclonal antibody against doxycycline for immunoassay of seven tetracyclines in bovine muscle and milk. *J Environ Sci Heal Part B* 48:92–100. <https://doi.org/10.1080/03601234.2013.726856>
- [18] Sattayasamitsathit S, Thavarungkul P, Kanatharana P (2007) Bismuth film electrode for analysis of tetracycline in flow injection system. *Electroanalysis* 19:502–505. <https://doi.org/10.1002/elan.200603726>
- [19] Calixto CMF, Cavalheiro ÉTG (2015) Determination of Tetracyclines in Bovine and Human Urine using a Graphite-Polyurethane Composite Electrode. *Anal Lett* 48:1454–1464
- [20] Calixto CMF, Cervini P, Cavalheiro ÉTG (2012) Determination of tetracycline in environmental water samples at a graphite-polyurethane composite electrode. *J Braz Chem Soc* 23:938–943. <https://doi.org/10.1590/S0103-50532012000500020>

- [21] Rajab Dizavandi Z, Aliakbar A, Sheykhani M (2017) A novel Pb-poly aminophenol glassy carbon electrode for determination of tetracycline by adsorptive differential pulse cathodic stripping voltammetry. *Electrochim Acta* 227:345–356. <https://doi.org/10.1016/j.electacta.2016.12.167>
- [22] Guo G, Zhao F, Xiao F, Zeng B (2009) Voltammetric determination of tetracycline by using multi-wall carbon nanotube - ionic liquid film coated glassy carbon electrode. *Int J Electrochem Sci* 4:1365–1372
- [23] Kesavan S, Kumar DR, Lee YR, Shim JJ (2017) Determination of tetracycline in the presence of major interference in human urine samples using polymelamine/electrochemically reduced graphene oxide modified electrode. *Sensors Actuators, B Chem* 241:455–465. <https://doi.org/10.1016/j.snb.2016.10.091>
- [24] Kushikawa RT, Silva MR, Angelo ACD, Teixeira MFS (2016) Construction of an electrochemical sensing platform based on platinum nanoparticles supported on carbon for tetracycline determination. *Sensors Actuators, B Chem* 228:207–213. <https://doi.org/10.1016/j.snb.2016.01.009>
- [25] Wong A, Scontri M, Materon EM et al (2015) Development and application of an electrochemical sensor modified with multi-walled carbon nanotubes and graphene oxide for the sensitive and selective detection of tetracycline. *J Electroanal Chem* 757:250–257. <https://doi.org/10.1016/j.jelechem.2015.10.001>
- [26] Allahverdiyeva S, Yardım Y, Şentürk Z (2021) Electrooxidation of tetracycline antibiotic demeclocycline at unmodified boron-doped diamond electrode and its enhancement determination in surfactant-containing media. *Talanta*. <https://doi.org/10.1016/j.talanta.2020.121695>
- [27] Taghioskoui M (2009) Trends in graphene research *Mater Today* 12:34–37. [https://doi.org/10.1016/S1369-7021\(09\)70274-3](https://doi.org/10.1016/S1369-7021(09)70274-3)
- [28] Tarcan R, Todor-Boer O, Petrovai I et al (2020) Reduced graphene oxide today. *J Mater Chem C* 8:1198–1224. <https://doi.org/10.1039/c9tc04916a>
- [29] Rowley-Neale SJ, Randviir EP, Abo Dena AS, Banks CE (2018) An overview of recent applications of reduced graphene oxide as a basis of electroanalytical sensing platforms. *Appl Mater Today* 10:218–226. <https://doi.org/10.1016/j.apmt.2017.11.010>
- [30] Liu H, Zhang L, Guo Y et al (2013) Reduction of graphene oxide to highly conductive graphene by Lawesson's reagent and its electrical applications. *J Mater Chem C* 1:3104–3109. <https://doi.org/10.1039/c3tc00067b>
- [31] Smith AT, LaChance AM, Zeng S et al (2019) Synthesis, properties, and applications of graphene oxide/reduced graphene oxide and their nanocomposites. *Nano Mater Sci* 1:31–47. <https://doi.org/10.1016/j.nanoms.2019.02.004>
- [32] Govindasamy M, Wang SF, Pan WC et al (2019) Facile sonochemical synthesis of perovskite-type SrTiO₃ nanocubes with reduced graphene oxide nanocatalyst for an enhanced electrochemical detection of α -amino acid (tryptophan). *Ultrason Sonochem* 56:193–199. <https://doi.org/10.1016/j.ultsonch.2019.04.004>
- [33] Govindasamy M, Wang SF, Subramanian B et al (2019) A novel electrochemical sensor for determination of DNA damage biomarker (8-hydroxy-2'-deoxyguanosine) in urine using sonochemically derived graphene oxide sheets covered zinc oxide flower modified electrode. *Ultrason Sonochem*. <https://doi.org/10.1016/j.ultsonch.2019.104622>
- [34] Jandaghi N, Jahani S, Kazemipour M et al (2019) One-pot synthesis of cerium doped 3D ZnO nano-flowers modified on glassy carbon electrode as portable electro-chemical sensing platform for sensitive detection of methotrexate as an anticancer drug. *Synth Met* 256:116119. <https://doi.org/10.1016/j.synthmet.2019.116119>
- [35] Ezhil Vilian AT, Kang SM, Yeong OhS et al (2020) A simple strategy for the synthesis of flower-like textures of Au-ZnO anchored carbon nanocomposite towards the high-performance electrochemical sensing of sunset yellow. *Food Chem* 323:126848. <https://doi.org/10.1016/j.foodchem.2020.126848>
- [36] Jain R, Thakur A, Kumar P, Pooja D (2018) Au/ZnO nanocomposites decorated ITO electrodes for voltammetric sensing of selenium in water. *Electrochim Acta* 290:291–302. <https://doi.org/10.1016/j.electacta.2018.09.061>
- [37] Marlinda AR, Pandikumar A, Yusoff N et al (2015) Electrochemical sensing of nitrite using a glassy carbon electrode modified with reduced functionalized graphene oxide decorated with flower-like zinc oxide. *Microchim Acta* 182:1113–1122. <https://doi.org/10.1007/s00604-014-1436-x>
- [38] Hummers WS, Offeman RE (1958) Preparation of Graphitic Oxide. *J Am Chem Soc* 80:1339. <https://doi.org/10.1021/ja01539a017>
- [39] Debbarma M, Das S, Saha M (2013) Effect of reducing agents on the structure of zinc oxide under microwave irradiation. *Adv Manuf* 1:183–186. <https://doi.org/10.1007/s40436-013-0020-7>
- [40] ICDD (2020). PDF-4+ 2021. International Centre for Diffraction Data, Newtown Square, PA, USA.
- [41] Degen T, Sadki M, Bron E et al (2014) The high score suite. *Powder Diffr* 29:S13–S18. <https://doi.org/10.1017/S0885715614000840>
- [42] Scherrer P (1918) Estimation of the Size and Internal Structure of Colloidal Particles by Means of Röntgen.

- Nachrichten von der Gesellschaft der Wissenschaften zu Göttingen 2:96–100
- [43] Periasamy M, Thirumalaikumar M (2000) Methods of enhancement of reactivity and selectivity of sodium borohydride for applications in organic synthesis. *J Organomet Chem* 609:137–151. [https://doi.org/10.1016/S0022-328X\(00\)00210-2](https://doi.org/10.1016/S0022-328X(00)00210-2)
- [44] Ferrari AC (2007) Raman spectroscopy of graphene and graphite: Disorder, electron-phonon coupling, doping and nonadiabatic effects. *Solid State Commun* 143:47–57. <https://doi.org/10.1016/j.ssc.2007.03.052>
- [45] Damen TC, Porto SPS, Tell B (1966) Raman Effect in ZnO. *Phys Rev* 142:570–573
- [46] Calleja JM, Cardona M (1977) Resonant Raman scattering in ZnO. *Phys Rev B* 16:3753–3761. <https://doi.org/10.1103/PhysRevB.16.3753>
- [47] Shin H-J, Kim KK, Benayad A, Yoon S-M, Park HK, Jung I-S, Jin MH, Jeong H-K, Kim JM, Jae-Young Choi YHL (2009) Efficient Reduction of Graphite Oxide by Sodium Borohydride and Its Effect on Electrical Conductance. *Adv Funct Mater* 19:1987–1992
- [48] Liu G, Wang L, Wang B et al (2015) A reduced graphene oxide modified metallic cobalt composite with superior electrochemical performance for supercapacitors. *RSC Adv* 5:63553–63560. <https://doi.org/10.1039/c5ra09748g>
- [49] Gomez-Alvarez MA, Morales C, Méndez J et al (2020) A Comparative Study of the ZnO Growth on Graphene and Graphene Oxide: The Role of the Initial Oxidation State of Carbon. *The Role of the Initial Oxidation State of Carbon C* 6(2):41. <https://doi.org/10.3390/c6020041>
- [50] Lesiak B, Kövér L, Tóth J et al (2018) C sp²/sp³ hybridisations in carbon nanomaterials – XPS and (X)AES study. *Appl Surf Sci* 452:223–231. <https://doi.org/10.1016/j.apsusc.2018.04.269>
- [51] Tay YY, Li S (2006) Size dependence of Zn 2p 3/2 binding energy in nanocrystalline ZnO. *Appl Phys* 88(17):173118. <https://doi.org/10.1063/1.2198821>
- [52] Moretti G (1998) Auger parameter and Wagner plot in the characterization of chemical states by X-ray photoelectron spectroscopy: A review. *J Electron Spectrosc Relat Phenom* 95(2–3):95–144. [https://doi.org/10.1016/S0368-2048\(98\)00249-7](https://doi.org/10.1016/S0368-2048(98)00249-7)
- [53] Sutar DS, Kushwaha N, Appani SK, Major SS (2020) Energy level alignment of graphene oxide and its derivatives with ZnO. *J Electron Spectrosc Relat Phenom* 23:146953. <https://doi.org/10.1016/j.elspec.2020.146953>
- [54] Fortgang P, Tite T, Barnier V et al (2016) Robust Electrografting on Self-Organized 3D Graphene Electrodes. *ACS Appl Mater Interfaces* 8:1424–1433. <https://doi.org/10.1021/acsami.5b10647>
- [55] Stojanović ZS, Đurović AD, Ashrafi AM et al (2020) Highly sensitive simultaneous electrochemical determination of reduced and oxidized glutathione in urine samples using antimony trioxide modified carbon paste electrode. *Sensors Actuators, B Chem*. <https://doi.org/10.1016/j.snb.2020.128141>
- [56] Wang H, Robinson JT, Diankov G, Dai H (2010) Nanocrystal growth on graphene with various degrees of oxidation. *J Am Chem Soc* 132:3270–3271. <https://doi.org/10.1021/ja100329d>
- [57] Huang HP, Zhu JJ (2011) Preparation of novel carbon-based nanomaterial of graphene and its applications electrochemistry. *Fenxi Huaxue/ Chinese J Anal Chem* 39:963–971. [https://doi.org/10.1016/S1872-2040\(10\)60450-1](https://doi.org/10.1016/S1872-2040(10)60450-1)
- [58] Vega D, Agüí L, González-Cortés A et al (2007) Voltammetry and amperometric detection of tetracyclines at multi-wall carbon nanotube modified electrodes. *Anal Bioanal Chem* 389:951–958. <https://doi.org/10.1007/s00216-007-1505-7>
- [59] European Medicines Agency (1995) VALIDATION OF ANALYTICAL PROCEDURES: TEXT AND METHODOLOGY Q2(R1). Eur Med Agency 1–15

Publisher's Note Springer Nature remains neutral with regard to jurisdictional claims in published maps and institutional affiliations.